TU Delft

Delft University of Technology

Document Version
Final published version

Licence
CC BY

Citation (APA)
Del Zoppo, M., Melo, J., Rossetto, T., Arêde, A., Di Ludovico, M., Prota, A., & Varum, H. (2026). Quasi-static flow-type loading tests for the out of plane performance assessment of full-scale masonry infill walls in reinforced concrete frames. *Engineering Structures*, *367*, Article 123663. https://doi.org/10.1016/j.engstruct.2026.123663

Important note
To cite this publication, please use the final published version (if applicable).
Please check the document version above.

Copyright
In case the licence states “Dutch Copyright Act (Article 25fa)”, this publication was made available Green Open Access via the TU Delft Institutional Repository pursuant to Dutch Copyright Act (Article 25fa, the Taverne amendment). This provision does not affect copyright ownership.
Unless copyright is transferred by contract or statute, it remains with the copyright holder.

Sharing and reuse
Other than for strictly personal use, it is not permitted to download, forward or distribute the text or part of it, without the consent of the author(s) and/or copyright holder(s), unless the work is under an open content license such as Creative Commons.

Takedown policy
Please contact us and provide details if you believe this document breaches copyrights.
We will remove access to the work immediately and investigate your claim.

This work is downloaded from Delft University of Technology.

Engineering Structures 367 (2026) 123663

Contents lists available at ScienceDirect

Engineering Structures

journal homepage: www.elsevier.com/locate/engstruct

Quasi-static flow-type loading tests for the out of plane performance assessment of full-scale masonry infill walls in reinforced concrete frames

Marta Del Zoppo [a,b,*], José Melo [c], Tiziana Rossetto [d,b], Antonio Arêde [c], Marco Di Ludovico [a], Andrea Prota [a], Humberto Varum [c]

[a] Department of Structures for Engineering and Architecture, University of Naples Federico II, Italy
[b] CEGE, University College London, UK
[c] CONSTRUCT, Faculty of Engineering, University of Porto, Portugal
[d] Department of Hydraulic Engineering, TUDelft, The Netherlands

ARTICLE INFO

Keywords:
Out of plane capacity
Masonry infill walls
Coastal flooding
Tsunami
Vulnerability assessment
Fragility analysis

ABSTRACT

Existing performance assessment methods for structures subjected to flow-type loading (i.e., flood, tsunami) rely on assumptions and previous knowledge derived from other hazards, such as earthquakes. However, flow-type induced loads on structures are fundamentally different in nature from seismic action, inducing long-duration non-uniform pressures on inundated components. Flume or wave basin tests on large-scale structural components under fluid loading are limited due to the difficulties in scaling. The present paper proposes a novel quasi-static testing method for performing full-scale tests on masonry infill walls in reinforced concrete (RC) frames subjected to simulated flow-type loading in a structural laboratory setting. The innovative test set up involves the use of an array of 28 pneumatic actuators and a novel testing procedure (i.e. test set-up and load protocols) is developed for simulating quasi-statically flow-type induced loads with increasing flow depth on full-scale building components. The feasibility of the proposed testing method is herein demonstrated on four full-scale masonry infill walls (dimensions 4.2 m x 2.3 m) in RC frames. The tests allow for the out of plane (OOP) performance of masonry infill walls to be assessed under flow-type loading conditions with increasing flow depth. Masonry walls are tested with and without plaster to point out the effect of the latter on the overall capacity of the wall. Original experimental data from flow-type testing are presented and discussed to provide insights into the OOP capacity of infill walls under flow-type loading. Finally, the OOP performance of infill walls under flow-type loading is compared with that of the same specimen previously tested under seismic loading conditions. Results attest the feasibility of the proposed testing method to characterise the structural response of full-scale building components under flow-type loading.

1. Introduction

The increasing number of natural disasters affecting coastal communities worldwide is pushing researchers to develop tools able to predict their impact and loss. In recognition of the high impact on the urban environment of tsunami and coastal flooding events, in the last 50 years there have been many significant experimental and numerical research programmes aimed at advancing inundation modelling capacity and understanding of inundation interaction with buildings 1–4, among others]. The latter have, however, mainly focused on the characterisation of fluid loading on buildings, and progress on the development of tools and methods for the characterisation of building response under flow-type loading is more recent.

Until the Tohoku Earthquake and Tsunami in 2011, published works that presented building performance assessments for tsunami via numerical analysis all adopted the same modelling strategies used in earthquake engineering [5,6]. More recently, a non-linear static analysis technique has been proposed, called the Variable Depth Pushover (VDPO) [7,8], for the structural analysis of buildings under flow-type loading that is now a recommended approach to tsunami structural analysis in the ASCE 7–22 [9]. A similar analysis technique, called the Incremental Flood Height analysis (IFHA), has been proposed for flood structural analysis of masonry buildings [10]. Despite the advancement in numerical analysis approaches for structural response prediction,

* Corresponding author at: Department of Structures for Engineering and Architecture, University of Naples Federico II, Italy.
E-mail address: marta.delzoppo@unina.it (M. Del Zoppo).

https://doi.org/10.1016/j.engstruct.2026.123663
Received 18 March 2026; Received in revised form 20 July 2026; Accepted 26 August 2026
Available online 3 September 2026
0141-0296/© 2026 The Authors. Published by Elsevier Ltd. This is an open access article under the CC BY license (http://creativecommons.org/licenses/by/4.0/).

these have never been validated with experimental data. This is because, tsunami and flood simulators in flumes or basins are primarily designed to investigate the hydraulic characteristics of flows and hence reproduce their actions on buildings at scales between 1:6–1:100 [11–13], that are too small to study the structural response of building models to these loads. Hydraulic tests performed with the biggest tsunami simulator in the world, located at PARI (Port and Airport Research Institute, Japan), were conducted on two 1:10 scaled reinforced concrete (RC) frames [14] and three 1:20 scaled shear walls [15]. However, the small scale of the specimens, governed by the capacity of the hydraulic test facility, still does not allow for a reliable assessment of the global and local (element-level) structure response, nor to produce data for the validation of numerical models. The absence of large-scale experimental data and of feasible experimental techniques for understanding the physical behaviour of buildings impacted by flow-type loads represents an important gap in the development of reliable numerical models for the fragility assessment of structures for tsunami and flooding, and a critical deficiency of international codes provisions for the design of buildings under flow-type loading.

The present study proposes a novel quasi-static testing method for performing full-scale tests on building components subjected to simulated flow-type loading in a structural laboratory setting. Realistic quasi-static simulations of tsunami induced loads on structures have never been attempted outside a hydraulic flume environment. However, hydraulic experiments simulating tsunami-like long period waves demonstrated that such unsteady flow conditions can be considered as quasi-steady in the context of structural analysis due to the small temporal variation of the flow with respect to the length scale of buildings [7,11]. The quasi-static testing method well-represent the quasi-steady and long duration characteristics of tsunami flow loading on buildings [11]. The test aims at simulating, in a static way, the hydrostatic and hydrodynamic pressure induced on buildings by the tsunami flow. The simulation of other tsunami-induced effects on structures, such as impact loads, is out of the scope of such testing approach. The novel testing procedure is implemented by modifying the advanced test set-up conceived at University of Porto (Portugal) for seismic tests (i.e., uniform pressure) [16,17], consisting of an array of 28 pneumatic actuators covering a surface of 4.2 m x 2.3 m, and potentially able to simulate complex distributed load patterns. The paper presents the experimental setup and load protocols conceived to perform flow-type quasi-static testing on building components. In essence, the experimental test simulates the Variable Depth Pushover analysis (VDPO), which means a flow-type load with monotonically increasing flow depth up to failure of the specimen. Equations to derive the normalised load protocols are presented to facilitate the test replicability.

The feasibility of the proposed experimental approach is demonstrated by testing four full-scale masonry infill walls in RC frames. Indeed, it has been demonstrated that infill walls, typical enclosures in Mediterranean regions, play a critical role in the evaluation of loads on structural elements during a flood or a tsunami [18,19]. Several experimental studies have been conducted so far to characterize the out-of-plane (OOP) response of masonry walls under quasi-static seismic loading conditions 20–22, among others]. However, the non-uniform load distribution of flow-type loads does not allow a direct use of such empirical models for the flood and tsunami cases. Full-scale experimental tests are herein conducted to investigate the OOP performance of masonry infill walls with different configurations (i.e., bare, with plaster) under different flow-type loading conditions (i.e., hydrostatic, combined hydrostatic and hydrodynamic). The experimental results are presented and discussed, focusing on the OOP crack pattern evolution and capacity at failure of masonry infill walls in RC frames. Obtained data are finally compared with a previous experiment conducted by Furtado [23] on a similar specimen under seismic (i.e., uniform) cyclic loading condition to point out the effect of the different loading patterns.

2. Flow-type testing facility and loading conditions

To perform quasi-static flow-type loading tests on full-scale building components, an existing test setup at University of Porto for the OOP testing of infill walls has been enhanced. Load protocols have been derived to simulate different flow-type loading conditions in agreement with a VDPO approach where the flow depth is monotonically increased up until failure of the specimen, assuming a constant Froude number [7]. The following sections discuss in detail the proposed setup and load protocols for flow-type testing.

2.1. Experimental setup and instrumentation

The specimen designed for the OOP tests consists of a full-scale one-bay one-storey RC frame with a masonry infill wall. The RC frame has the only role of creating the boundary condition for the infill wall and to allow the OOP loads monitoring during the test, as better discussed in the following.

The set-up adopted for the OOP experimental campaign is depicted in Fig. 1 and consists of 28 pneumatic actuators arranged in four horizontal lines in x direction (horizontal in-plane), with wood plates placed between the actuators and the specimen to uniformly distribute the load. The setup is able to cover a surface of 4.2 m x 2.3 m. The pneumatic actuators are supported by a steel reaction frame, which is a self-equilibrated structure designed with a concept similar to that used in previous experimental campaigns [16,17,24]. The flow-type loading is applied over the out-of-plane z direction (see Fig. 1), orthogonal to the wall panel, to assess the OOP performance. The steel structure is connected to the RC frame by steel bars at 14 points (5 on the bottom beam, 5 on the top beam, and 2 at middle-height of each column), as shown in Fig. 2 (label L). The steel bars are coupled with 14 load cells that allow the monitoring of RC reaction forces and, hence, the OOP loading during the test. It should be noted that only the masonry infill wall is directly loaded during the test, and no OOP or axial load is applied to the surrounding RC frame. The RC frame is connected to the outer steel frame at the base of each RC column by two vertical tie rods and one horizontal adjustable steel cylinder, and at the top beam in two points to block the transversal displacement of the beam (Fig. 1). The mid-span of top and bottom beams is free to move in the vertical direction.

In the original setup configuration, all actuators were controlled by the same input to generate a uniform load distribution over the entire surface of the specimen, simulating a seismic loading. To perform the flow-type testing, the control system of the original setup has been modified to make each line of actuators independent from the others such that the array of actuators is able to simulate the varied load distributions needed to simulate an increasing flow depth level.

To monitor the OOP deformation of the walls, 27 LVDTs are placed over the specimen, as shown in Fig. 2 (labels A to F). Six additional LVDTs (i.e., G1-G5 and I1) are installed on the RC beams and columns, to ensure negligible OOP deformation of the RC frame in the z direction (out-of-plane). The vertical displacement (i.e., y direction vertical in-plane) of the top beam is also monitored by one LVDT (i.e., G6) placed in the middle span of the beam.

2.2. Load protocols for flow-type loading

Quasi-static structural tests are typically performed under displacement control; however, flow-type pressures are force-controlled depending primarily on flow depth and velocity. Hence, force-based load protocols are derived to perform the flow-type quasi-static testing.

The hydrodynamic (i.e. drag) loading induced by the flow is computed following the empirically validated equations proposed by Foster et al., 2017 [11] for steady flows. The drag force formulation depends on the flow regime at the building, which is described by the Froude number of the impacting flow (i.e. $Fr = u/\sqrt{gH_w}$, with u the flow

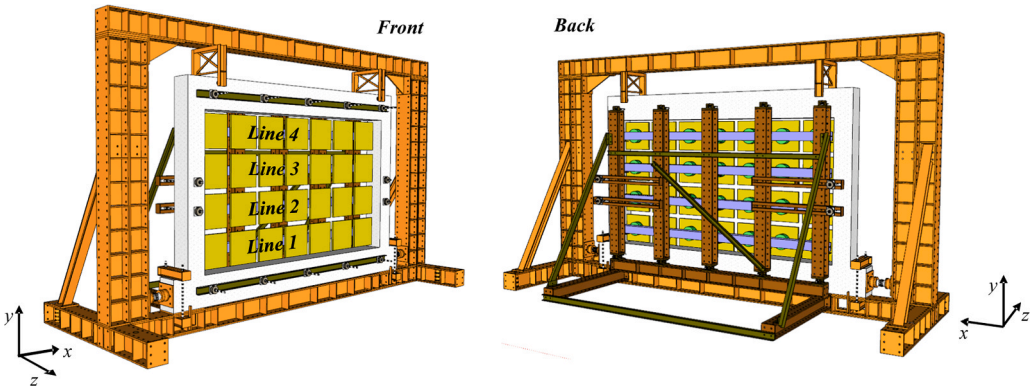

Fig. 1. Test set-up, front and back view.

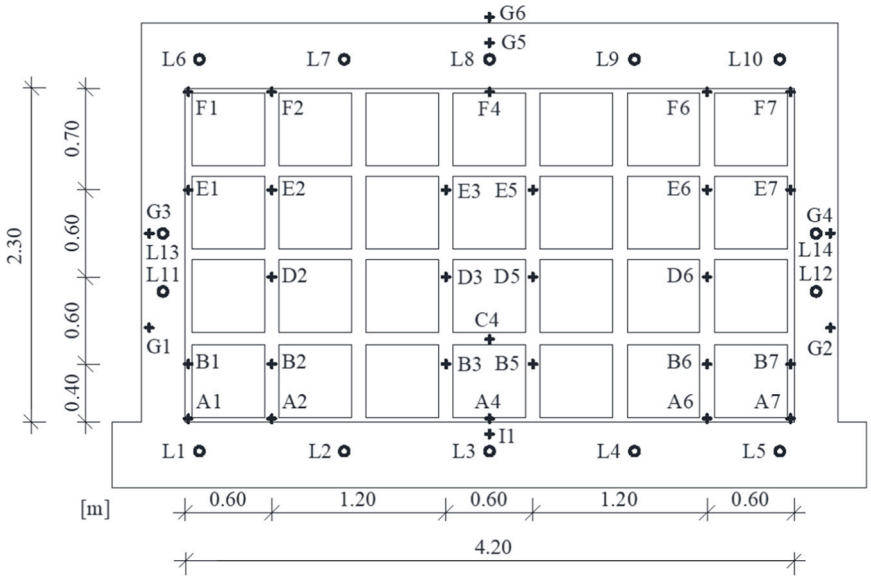

Fig. 2. Load cells (L) and LVDTs (A-I) layout, back view (dimensions in m).

velocity, g the gravitational acceleration and H_w the flow depth). When Fr is less than a critical value, Fr,c, the flow regime is subcritical and the flow depth at the front and back of the building is similar; for $Fr > Fr$,c, the flow condition is choked, there is a significant lowering of the flow depth at the back of the building with respect to the front, and a hydraulic jump forms downstream. According to Foster et al., the net drag force acting on a rectangular surface of width b is:

$$F_D = \begin{cases} 0.5 C_D \rho u^2 H_w\, b & \text{if } \mathrm{Fr} < \mathrm{Fr,c} \\ \lambda_s \rho g^{1/3} u^{4/3} H_w{}^{4/3} b & \text{if } \mathrm{Fr} \geq \mathrm{Fr,c} \end{cases} \quad (2)$$

where ρ is the sea water density (assumed here to be 1.2 t/m^3 to account for suspended sediment [7]), C_D is the drag coefficient, and λ_s is the leading coefficient for steady flows, computed as a function of the blocking ratio, b/w, as follows:

$$\lambda_s = 0.73 + 1.2(b/w) + 1.1(b/w)^2 \quad (3)$$

For this application, a blocking ratio $b/w = 0.6$ is adopted for computing the flow-type loading, to reflect the conditions of a dense urban area. However, different values of b/w can be considered based on the literature to reflect different built environment conditions. The net drag force on the specimen is computed according to Eq. 2 and then converted into a uniform horizontal pressure distribution acting on the portion of wall below the flow depth H_w.

The unbalanced hydrostatic loading, that acts on façade infill walls, is conventionally computed as $F_S = 0.5\rho g {H_w}^2 b$, and it is converted into a triangular pressure distribution acting on the portion of wall below the flow depth H_w.

Fig. 3a shows the variation of drag and hydrostatic forces as a function of the flow depth on a portion of exterior infill wall of width b = 60 cm. The drag force is computed for different Froude numbers (i.e., 0.5, 0.8 and 1.0) to point out the relative magnitudes of the two components of the flow-type loading.

The hydrostatic and hydrodynamic pressure distributions acting in z direction on the exterior side of the masonry infill wall are discretized into four-point loads over the height of the wall (i.e., y direction) to meet the setup configuration, as shown in Fig. 3b (from F_1 at the bottom line of actuators to F_4 at the top). A different setup layout with additional horizontal lines of actuators may lead to more refined load discretization and, hence, different loading protocols. The approach selected for the flow-type loading discretization into four time-histories is a function of the flow depth, H_w, as follows:

- for values of H_w lower than the centroid for Line 2 of actuators, only F_1 is non-null while the other lines actuators are not activated;
- for values of H_w lower than the centroid for Line 3 of actuators, F_1 and F_2 are non-null while the other lines actuators are not activated;
- for values of H_w lower than the centroid for Line 4 of actuators, F_1, F_2 and F_3 are non-null while fourth line is not activated;

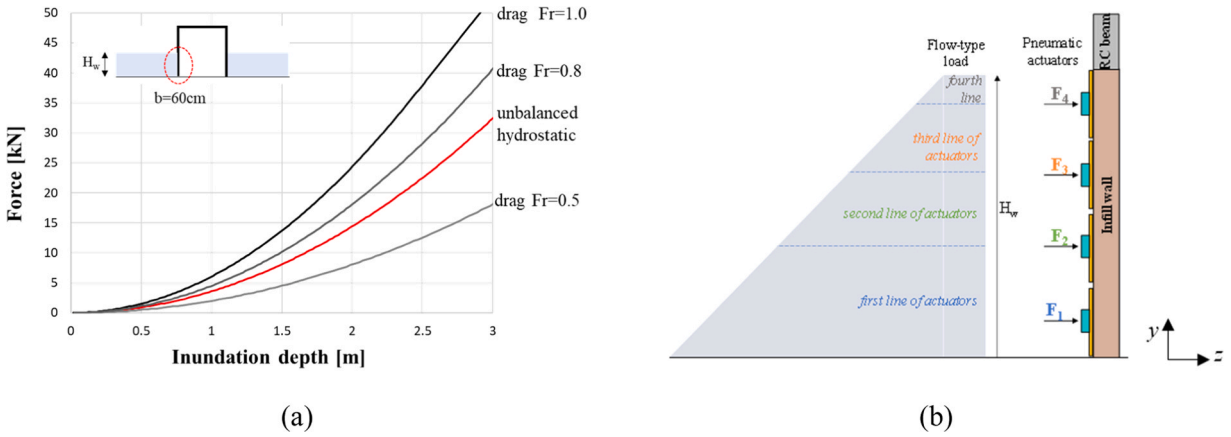

Fig. 3. Flow-type load components (a) and loading scheme for the flow-type experimental tests (b).

- for values of H_w greater than the centroid of Line 4 of actuators, all four lines are activated.

For each flow depth value, the four forces equivalent to the actual pressure distribution in z direction of the specimen are computed in order to produce the same external work on the panel, assuming an OOP vertical arch mechanism with crack line between F_2 and F_3. This leads to four force time histories for each loading condition (i.e., hydrostatic only and combined hydrostatic-hydrodynamic with Froude number equal to 0.6, 0.7, 0.8, 0.9 and 1.0).

To comply with the experimental needs, normalised load protocols are then derived to be implemented into the control system. In detail: (*i*) threshold values are defined for F_1 to activate the second, third and fourth lines of actuators, (*ii*) a correlation law between F_1 and the other forces (i.e. F_2-F_4) is derived to replicate the flow-type load distribution for an increasing flow depth, (*iii*) the protocols are normalised with respect to the impacting surface b to accommodate specimens with different dimensions, and (*iv*) the protocols simulate two flow-type loading conditions, that are flood (i.e., hydrostatic only) and tsunami (i.e., combined hydrostatic-hydrodynamic).

For the definition of the load protocols, two actuators' arrangements are considered, as shown in Fig. 4: Configuration 1, where all the actuators are equally spaced, and the wood plates have dimensions 0.5 m × 0.5 m; Configuration 2, where the first line of wood plates have dimensions 0.3 m × 0.5 m while the fourth line have dimensions 0.7 m × 0.5 m. Configuration 2 allows for the activation of the second line of actuators at a lower value of F_1 with respect to Configuration 1.

To derive the load protocols, the actual hydrostatic and hydrodynamic pressure distributions acting over the specimen have been calculated for flow depth varying from 0 to 4 m with step 0.1 m, and for Froude numbers from 0.6 to 1.0. The pressure distributions corresponding to each flow depth level are then converted into four forces acting in z direction, as previously discussed. Based on such data, a simple expression to compute the normalised threshold values for F_1 is derived as a function of the impacting surface and of the flow condition (hydrostatic or combined). In detail, the thresholds represent the normalised values of F_1 at which the second, third and fourth lines of actuators start activating, respectively. The expression derived for the threshold values is reported here:

$$F_{1\text{-}n} = k_n F_{s,1\text{-}n} b \tag{4}$$

where $F_{1\text{-}n}$ is the value of F_1 at which line n is activated, $F_{s,1\text{-}n}$ is the hydrostatic component of F_1 at which line n is activated (see Table 1), b is the impacting surface width and k_n is a calibrated parameter which equals 1 for hydrostatic loading and is a function of the Froude number, Fr, for the tsunami case, as reported in Table 1.

The trend of the coefficient k_n as a function of the Froude number is

Table 1
Normalised threshold values of F_1 in a single actuator for the3 activation of second, third and fourth lines of actuators.

	Setup Configuration 1		Setup Configuration 2	
Actuators	$F_{s,1\text{-}n}$	k_n	$F_{s,1\text{-}n}$	k_n
Second line, n = 2	6 kN/m	2.36 Fr + 0.20	5 kN/m	2.10 Fr + 0.25
Third line, n = 3	14 kN/m	1.63 Fr + 0.50	12 kN/m	1.54 Fr + 0.53
Fourth line, n = 4	23 kN/m	43. Fr + 0.60	21 kN/m	1.27 Fr + 0.67

*with Fr between 0.6 and 1.0.

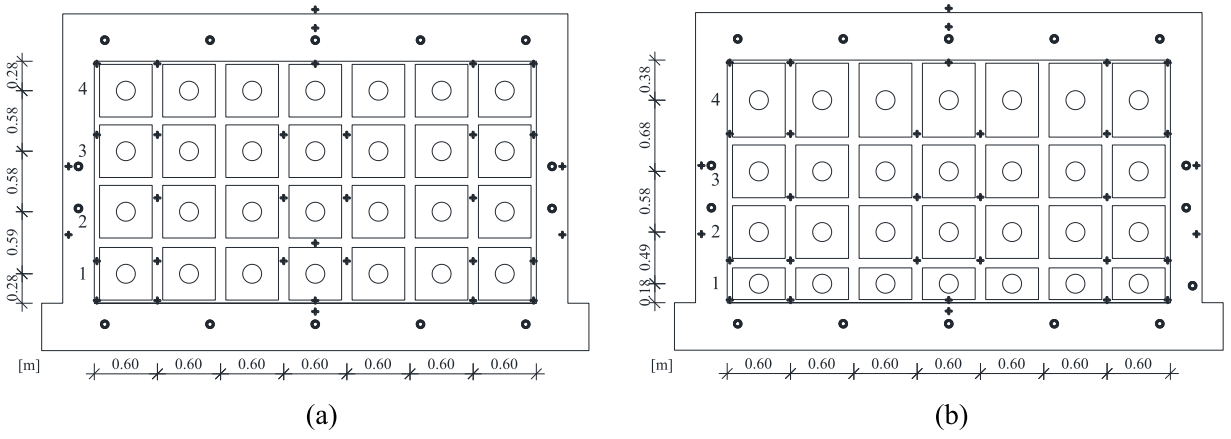

Fig. 4. Actuators Configuration 1 (a) and Configuration 2 (b).

shown in Fig. 5 for the three lines of actuators. The plots show an almost linear trend of k_n for the range of *Fr* herein investigated; the expressions of k_n reported in Table 1 are hence derived by linear regression.

Table 2 reports the triggering values of F_1 computed for Configuration 1 and for different Froude numbers, assuming the surface of the impacted element $b = 4.2$ m. For instance, for a tsunami withFr = 0.6, the second line of actuators is activated when F_1 reaches 40.7 kN, the third line is activated when F_1 is 86.9 kN and the fourth line when F_1 is 140.8 kN. In case of flood loading conditions, the second, third and fourth lines of actuators are activated when F_1 reaches 25.2 kN, 58.8 kN and 96.6 kN, respectively.

During the test, the force F_1 increases monotonically. Conversely, once activated, the generic *n*-line of actuators cannot be increased monotonically as in the case of F_1. Instead, the actuator forces follow the actual relationship between F_n and F_1 according to the real load pattern distribution. For the sake of simplicity, the generic force F_n is herein expressed as a function of F_1 by means of a coefficient α_n, where:

$$F_n = \alpha_n F_1 \tag{5}$$

Fig. 6a shows the trend of coefficient α_n as a function of F_1 normalised by the impacting surface width *b* for hydrostatic flow and for combined flow with different Froude numbers. Removing the triggering force value, $F_{1\text{-}n}$, it is observed that the trend of α_n is linear for the first branch of the curve and then follows a logarithmic equation, as depicted in Fig. 6b-d. The Froude number is observed to only slightly affect the trend of α_n. Hence, for the tsunami flow condition, the mean curve of α_n is considered for each line of actuators and the expression of α_n is then derived by regression. A similar approach is followed to define the curves of the hydrostatic flow condition. The derived regression coefficients λ_n, β_n and γ_n are summarized in Table 3 for the different flow condition and setup configurations. The general expression of α_n is reported below and is highlighted in red in Fig. 6b-d:

$$\alpha_n = \min \begin{cases} \lambda_n (F_1 - F_{1-n})/b \\ \beta_n \ln((F_1 - F_{1-n})/b) + \gamma_n \end{cases} \tag{6}$$

A control script has been written to implement the new load protocols into the displacement control testing condition. The overall test is displacement controlled with a constant velocity equal to 0.03 mm/s to reach the triggering forces at Line 1, and the force in the other three lines of actuators are consequently scaled according to Eq. 5. For safety reasons the OOP displacement is controlled for the entire duration of the test by means of LVDT C4 (Fig. 2). Being the flow-type loading based on force protocols, they are applicable up to the achievement of peak OOP capacity. In the post-peak phase, the test is switched into a uniform OOP displacement applied over the entire wall, monotonically increasing up to complete breakaway failure. Such post-peak phase aims at simulating a flow depth greater than the height of the infill wall to catch the complete damage mechanism.

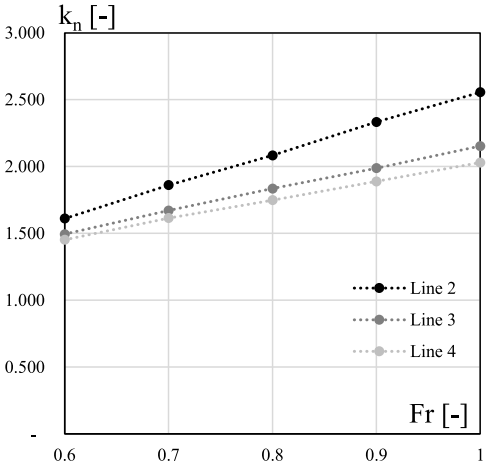

Fig. 5. Trend of coefficient k_n.

3. Tests program

The tests program consists of four identical single-layer masonry infill walls in RC frames. The specimens are representative of existing buildings in the Mediterranean region, like Italy and Portugal. The same specimen designs were already tested under different configurations [16,17,23,24]. It should be noted that only the infill walls were loaded, while the surrounding frame provided the real restraint conditions.

The specimens are tested in different configurations, as also summarized in Table 4:

1. OOP_01: Bare infill wall subject to flood (i.e. hydrostatic load only)
2. OOP_02: Bare infill wall subject to tsunami withFr = 0.6
3. OOP_03: Infill wall with plaster (mortar) subject to tsunami withFr = 0.6
4. OOP_04: Infill wall with plaster (mortar and non-structural grid) subject to tsunami withFr = 0.6

Two different flow-type loading conditions are considered to assess the effect of the hydrostatic and hydrodynamic load components. Specimen OOP_01 is tested under hydrostatic load only, simulating a flood condition. The remaining specimens are tested under combined hydrostatic and hydrodynamic loading, simulating a tsunami with *Fr* = 0.6. Given the limited capacity of the pneumatic actuators, Froude numbers greater than 0.6 could not be simulated with the current setup to achieve the out-of-plane collapse of the specimens.

The walls are tested in their bare configuration, as well as in the more realistic condition with plaster on both sides. For the plaster, two different typologies of plasters are considered: a plaster with only mortar, and a plaster with a non-structural grid to prevent undesired shrinkage cracks of the mortar. It should be noted that the latter does not represent a strengthening solution for the infill wall, such as a FRCM system (Fibre Reinforced Cement Matrix), given the non-structural properties of the grid.

The specimens are built in sequence. Following the end of each test, the remaining parts of the wall are removed, and a new infill wall is built inside the existing RC frame. The creation of each wall takes 2–3 days, and the testing is performed after at least 28 days to allow the curing of the mortar.

In the next sections, details of the specimens geometric and mechanical properties are reported, as well as their calculated capacity (pre-test) under different loading conditions.

3.1. Geometry of specimens

The full-scale RC frame is designed according to Eurocode 8 – Part 1 [25] and built in the laboratory, see structural details in Fig. 7a. The column dimensions are 0.30 m × 0.30 m while the beam cross-section dimensions are 0.30 m × 0.50 m. The single-leaf infill wall dimensions are 4.2 m × 2.3 m (width × height), and no gaps are left between the wall and the surrounding RC frame (i.e., four-edges boundary condition). No reinforcement is used to connect the infill panel to the RC frame. All the infill walls are built with horizontal hollow clay bricks with dimensions 150 mm × 200 mm × 300 mm (thickness × height × width), characterized by a void percentage equal to 58% (see Fig. 6b). Bed joints have an overall thickness of 10 mm. All the panels are built according to traditional construction methods, starting with the application of the first layer of 10 mm mortar joint (interface panel-bottom beam) and then placing the first brick next to the column. The proper filling of 10 mm vertical joint between the brick and the column is ensured. Construction of each infill panel up to the top row of bricks is conducted in one day. The last row of bricks is placed one day later, to ensure proper hardening and settlement of the mortar bed-joints and

Table 2
Threshold values of F_1 [kN] for the activation of upper lines assuming $b = 4.2$ m in Configuration 1.

	Flood	Tsunami Fr= 0.6	Tsunami Fr= 0.7	Tsunami Fr= 0.8	Tsunami Fr= 0.9	Tsunami Fr= 1.0
F1–2 [kN]	25.2	40.7	46.7	52.6	58.6	64.5
F1–3 [kN]	58.8	86.9	96.5	106.1	115.7	125.2
F1–4 [kN]	96.6	140.8	154.7	168.5	182.3	196.1

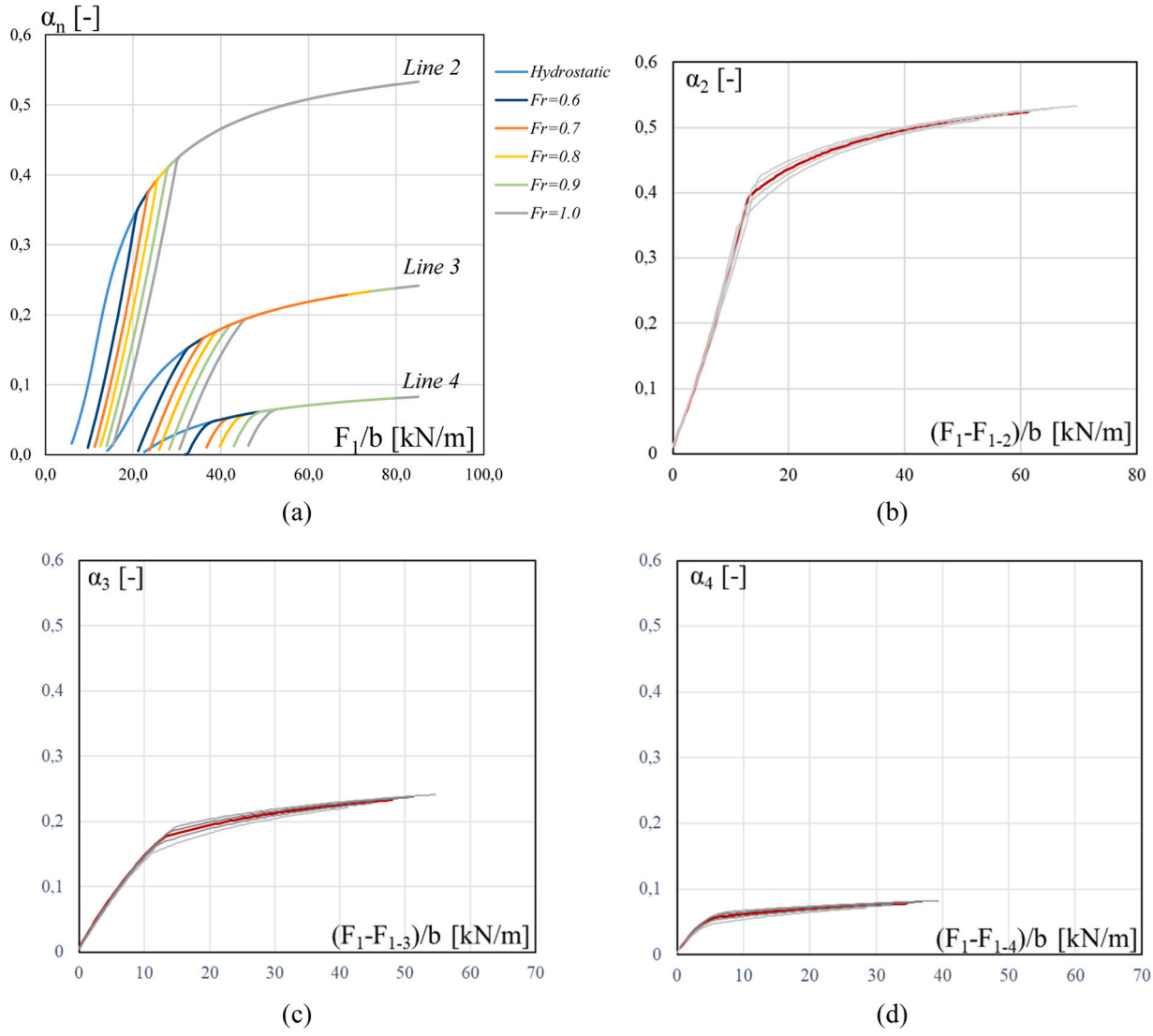

Fig. 6. Variation of the coefficient α_n (Configuration 1) for different lines of actuators.

Table 3
Parameters for the calculation of α_n.

	Actuators	Setup Configuration 1			Setup Configuration 2		
		λ_n	β_n	γ_n	λ_n	β_n	γ_n
Tsunami (Fr=0.6–1.0)	Second line, n = 2	0.029	0.082	0.19	0.043	0.095	0.25
	Third line, n = 3	0.013	0.044	0.06	0.015	0.067	0.07
	Fourth line, n = 4	0.008	0.013	0.03	0.007	0.022	0.04
Flood (hydrostatic)	Second line, n = 2	0.026	0.125	0.02	0.037	0.128	0.12
	Third line, n = 3	0.010	0.072	-0.05	0.015	0.100	-0.07
	Fourth line, n = 4	0.003	0.026	-0.02	0.005	0.039	-0.04

avoid possible shrinkage cracks. Due to the geometric configuration of the frame, it has been necessary to build the top row with half-height bricks and then fill the interface between the brick and the top beam with mortar.

The plaster is applied at least 7 days after the construction of the panel on both sides of the masonry infill wall, with a thickness of 10 mm.

Table 4
Test matrix.

Test ID	Setup Configuration	Loading condition	Plaster
OOP_01	2	Flood (hydrostatic)	no
OOP_02	1	Tsunami Fr = 0.6)	no
OOP_03	1	Tsunami Fr = 0.6)	Mortar
OOP_04	1	Tsunami Fr = 0.6)	Mortar + non-structural grid

The non-structural grid embedded in the plaster is made of glass FRP and is applied on both sides of the wall. No mechanical anchors are adopted, but the grid is applied both on the wall and the surrounding frame to strengthen the connection between infill wall and concrete.

3.1.1. *Mechanical properties of materials*

A regular C20/25 grade concrete is used to construct the RC frame, and B450C steel is used for the internal reinforcement. The mechanical characterization of the masonry walls was previously conducted by Furtado et al., 2020 [26] according to the standard EN 1052–1 [27] to perform compressive tests. Indeed, both the workmanship and the materials adopted for producing the specimens presented in the present study (purchased from the same batch) are the same of those used in the experimental campaign previously conducted by Furtado et al. (2020) [26]. Beside the different time of construction of the walls, the control on materials and workmanship allows to reduce uncertainties related to the construction process and material properties that could affect the OOP test results [28]. The mean compressive strength of three-brick masonry units perpendicular to the holes' direction is 1.09 MPa (*CoV* of 12.8%) while the elastic modulus has a mean value of 1975 MPa (*CoV* of 36.7%). The flexural strength parallel and perpendicular to horizontal bed joints are 0.139 MPa (*CoV* of 12.6%) and 0.322 MPa (*CoV* of 18.1%), respectively. Regarding the hollow clay bricks, the compressive strength perpendicular to the holes' direction provided by the supplier is 1.5 MPa.

An industrial pre-dosed M5 mortar is used to build the walls (i.e., bed joints) and for the plaster, with a thickness of 10 mm. The M5 mortar characterised by mean compressive and flexural strengths of 8.6 MPa and 5.1 MPa, respectively. The adoption of a low-strength M5 mortar is to better represent the typical mortar used in existing RC buildings in Mediterranean regions.

The non-structural glass fibre grid used for the reinforced plaster has a nominal square spacing of 10 mm, a density of 114 gr/m^2, nominal longitudinal and transverse tensile strengths of 32 kN/m and 29.2 kN/m respectively, and a strain at rupture of 4.9%.

4. Experimental results

The experimental results are herein discussed for each specimen in terms of observed crack pattern, failure mode and peak capacity. Fig. 8 summarizes the cracks' evolution for all specimens, and Fig. 9a,b report the experimental OOP force-displacement curves and the total OOP force over time for the four tests in the flow-type loading phase, respectively. The OOP displacement corresponds to records from the LVDT placed at 0.57 m from the base of the wall (see Fig. 2). As

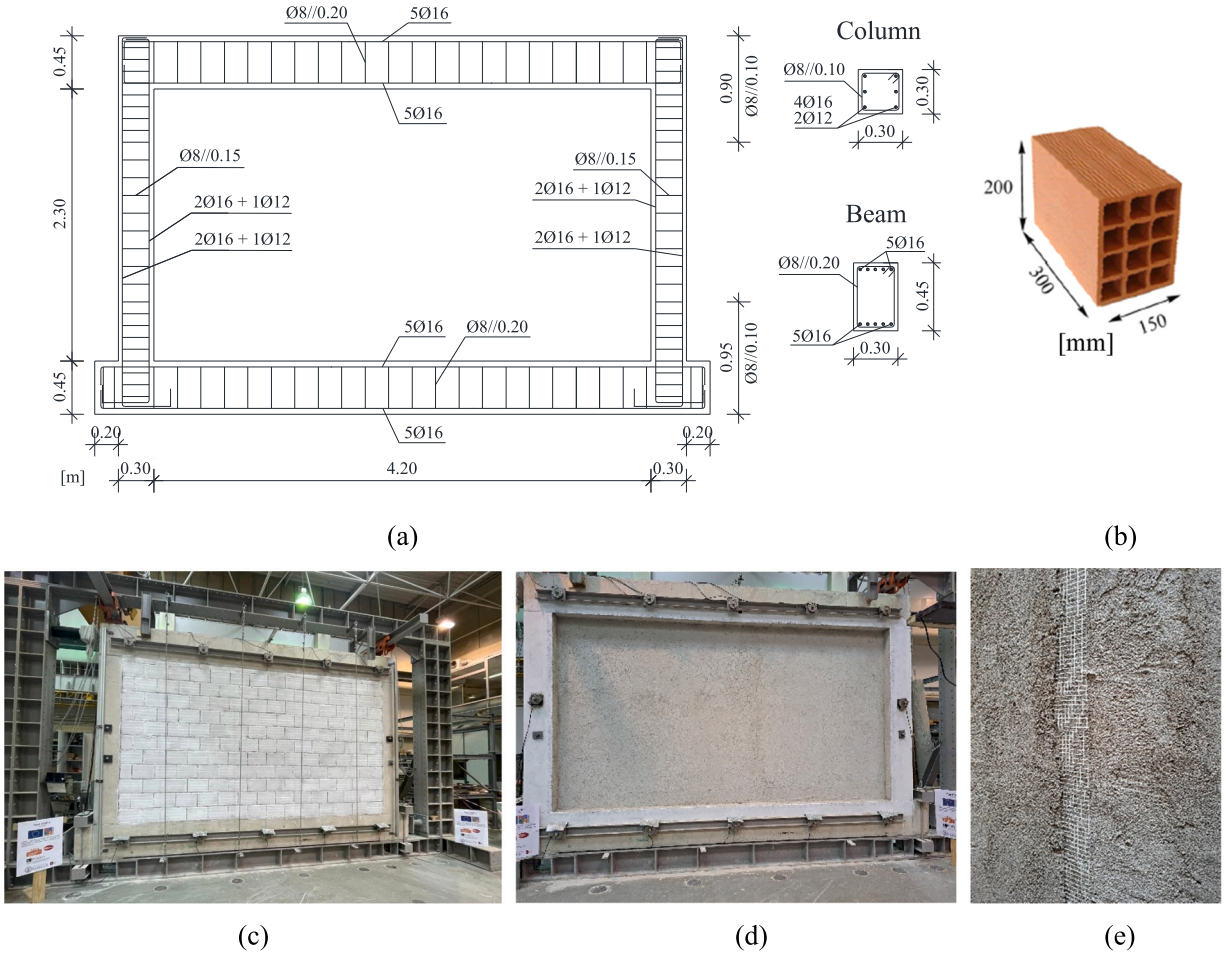

Fig. 7. RC frame details (a), bricks geometry (b), OOP_01-OOP_2 specimen front view (c), OOP_03-OOP_4 specimen front view (d), plaster with non-structural grid (e).



Fig. 8. Crack pattern evolution for tested specimens up to complete breakaway.

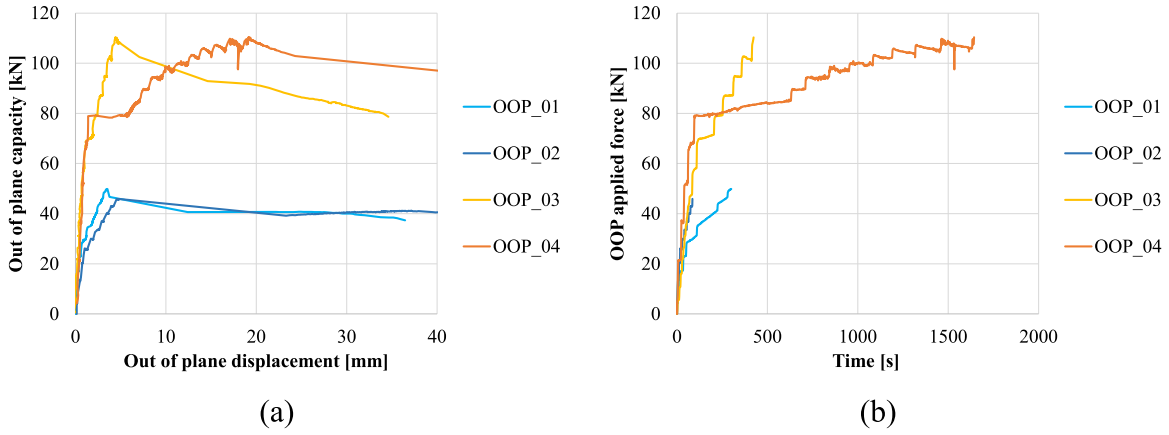

Fig. 9. Experimental OOP capacity curves for masonry infill walls under flow-type loads (a) and experimental total OOP force-time relationship during the flow-type phase (b).

previously mentioned, the overall OOP force is measured as the sum of the 14 load cells records over the RC frame. Such records represent the reaction of the RC frame to the OOP load applied on the infill wall. The match between reaction force and pneumatic actuators forces has been verified for all specimens, confirming a perfect connection and load transfer between masonry and concrete. To further analyse the OOP failure mechanism, Fig. 10 shows the OOP deformed shapes of the walls at peak capacity in the *x* and *y* directions. The deformation in *y* direction (i.e., vertical) is taken from LVDTs placed at the mid-span of the panel, while in *x* direction (i.e., horizontal) the deformation is derived from LVDTs placed at 0.4 m from the bottom of the wall.

4.1. OOP_01

The first test is conducted on the bare masonry wall under a flood (i.e., hydrostatic) loading condition, using setup Configuration 2 (Fig. 4) to reduce the force component on the first line of actuators and allow the activation of the second line before the failure. The initial concentrated loading on the lower row of bricks induces a first crushing of the bricks at the bottom of the wall, see Fig. 8 left. The deformed shape of the wall

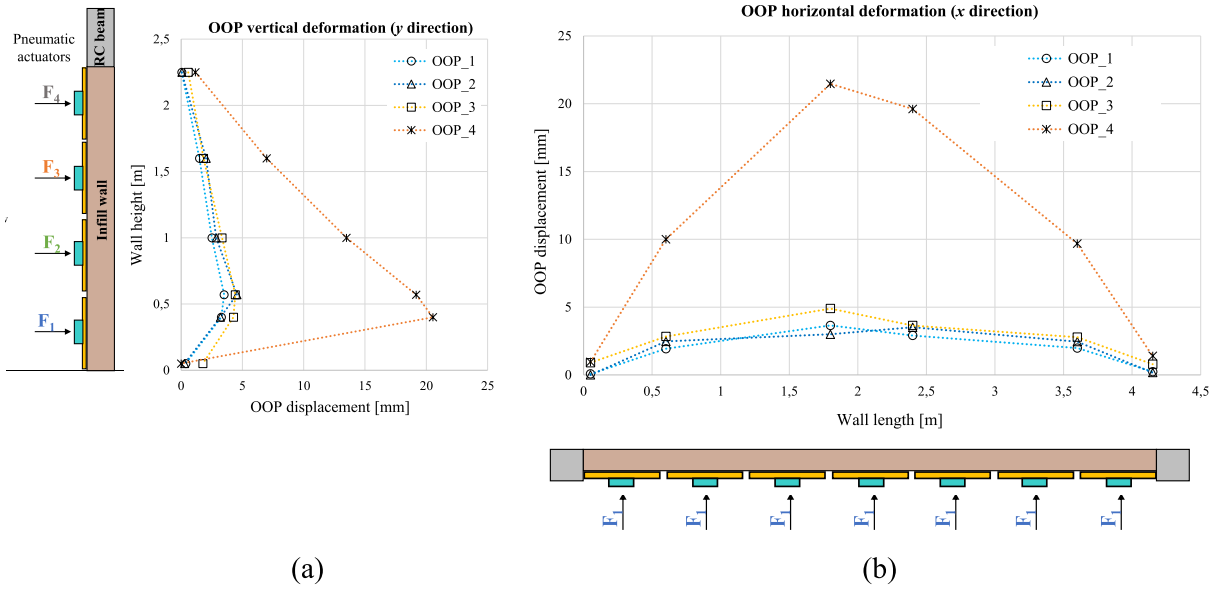

Fig. 10. OOP deformed shapes at peak capacity: (a) OOP deformation along a vertical line at mid-panel, (b) OOP deformation along a horizontal line at h= 0.4 m from the bottom of the panel.

shown in Fig. 10 indicates a higher OOP deformation at 0.57 m from the bottom of the wall. At this stage, the maximum OOP capacity of the wall is reached, corresponding to 49.9 kN. In the next phase of the test, the formation of a sub-horizontal crack line at about the mid-height of the wall is observed with the expulsion of the bricks below the crack. After this point, the flow-type phase is stopped and switched into a uniform OOP displacement distribution over the entire height of the panel to simulate the progressive damage caused by a flow depth equal to the height of the wall. At the end of the test, the complete expulsion of the masonry panel is reached. No visible cracks are recorded at the boundaries between masonry panel and RC frame before the OOP breakaway.

4.2. OOP_02

The second test is conducted on the bare masonry wall under a tsunami loading condition with a Froude number $Fr = 0.6$. The test is performed with the setup Configuration 1 to check any influence of the load application method on the overall damage evolution. The observed damage pattern and failure mode of OOP_02 are similar to those of specimen OOP_01, and the maximum capacity of the wall is reached at 45.9 kN with the first crushing of bricks at the bottom of the wall and the following partial OOP expulsion of the bricks. It is observed that the different setup configuration has a negligible effect on the overall performance and damage evolution of the tested specimens. For this reason, the tests on OOP_03 and OOP_04 are conducted with setup Configuration 1.

4.3. OOP_03

The third test is conducted on the masonry wall with plaster (i.e., mortar only) applied on both sides of the specimen under a tsunami loading condition with a $Fr = 0.6$. The application of the plaster does not affect the crack pattern evolution, as shown in Fig. 8. Indeed, damage is again observed at the bottom of the panel with the local crushing of the bricks, and the peak OOP capacity is reached at the same OOP displacement value of OOP_01 and OOP_02. The peak capacity is observed to increase to 110.3 kN due to the contribution of the plaster in compression to the flexural resisting mechanism. After the partial expulsion of the bottom part of the panel governed by a horizontal crack at the mid-height of the wall, the test is stopped and switched to a uniform displacement distribution up to the complete expulsion of the masonry panel. Also for test OOP_3, no visible cracks are recorded at the boundaries between masonry panel and RC frame.

4.4. OOP_04

The fourth test is conducted on the masonry wall with the plaster and non-structural grid on both sides of the specimen under a tsunami loading condition with $Fr = 0.6$. The crack pattern evolution reported in Fig. 8 clearly shows the effect of the non-structural grid on the damage of the masonry panel. Indeed, the grid prevents the partial OOP expulsion of the bricks and changes the overall crack pattern. The peak capacity is again reached due to the crushing of the bricks at the bottom of the wall. Then, the loss of connection between the bottom part of the masonry panel and the frame is observed. At the end of the test, after the application of the uniform OOP displacement over the entire height of the panel, the wall remains attached to the frame due to the anchorage provided by the grid. In terms of OOP capacity, specimen OOP_04 reached 110.4 kN, almost the same value as specimen OOP_03, confirming that the non-structural grid does not contribute in capacity but in crack control and damage limitation. This is confirmed by the fact that the peak capacity of specimen OOP_4 is reached at an OOP deformation level four to five times higher than other tests, as visible in Fig. 10. Such observations are compatible with the properties of the non-structural grid adopted for the plaster, that is not able to enhance the tensile and flexural capacity of the mortar. Indeed, the original role of the non-structural grid inside the plaster is to control the shrinkage and cracking of the mortar, avoiding stress concentrations.

5. Discussion

The four tests conducted with the novel quasi-static flow-type testing procedure provided a new understanding of the OOP performance of masonry infill walls restrained on four edges in RC frames under flow-type loading with increasing flow depth. In terms of crack pattern evolution, tests OOP_01, OOP_02 and OOP_03 experienced a similar damage evolution and crack pattern. Conversely, in OOP_04 the non-structural grid played a fundamental role in avoiding the complete breakaway of the wall. This reduces the formation of debris and the amount of water

passing inside the building.

The OOP capacity of infill walls under flow-type loading is governed by the bricks failure at the bottom of the wall due to the asymmetric vertical deformed shape of the panel, as shown in Fig. 10, that suggests the formation of an asymmetric vertical thrusting arch. In particular, the maximum OOP displacements of the walls are recorded at a distance 0.57 m from the base of the panel for OOP_1, 2 and 3, and 0.40 m from the base for OOP_4. The observed arching mechanism is related to the four-edges boundary conditions of the wall panel with respect to the surrounding RC frame. The damage observed after the peak due to the increasing flow level is not related to the actual resisting mechanism of the walls and could lead to misleading interpretation of the failure mode of the walls. To confirm this finding, the experimentally observed damage pattern is compared with field observations collected during an EEFIT (Earthquake Engineering Field Investigation Team) mission after the 2004 Indian Ocean Tsunami. Similar damage patterns are also highlighted in [29,30,31] on RC buildings in Indonesia, Thailand and Sri Lanka. Such RC buildings usually present masonry infill walls made by solid clay bricks or hollow concrete blocks, with or without plaster (mortar only). The pictures, reported in Fig. 11, confirm a good match between the observed and the simulated damage condition when the flow depth overcomes the height of the infill wall (i.e., breakaway condition). It should be noted that such damage pattern does not correspond to the actual OOP failure mechanism achieved by the masonry wall panel. Hence, the proposed experimental approach allows monitoring of the damage evolution during a flow-type loading, catching the real failure mechanism at peak capacity, which is hard to observe after a tsunami event. Such information is of paramount importance for defining damage levels in the context of damage and loss assessment for disaster risk management.

The load cells placed between the RC frame and the steel reaction frame allowed measurement of the RC frame horizontal (i.e., z direction) reaction during the tests and to estimate the distribution of loads transferred by the infill wall to beams and columns. Fig. 12 shows the ratio between transferred load to top/bottom beams and left/right columns and total OOP load during the tests. The records show that the bottom RC beam attracts about 60–70% of the total OOP load, while the top beam around 6% without plaster and 10% if plaster is applied. The two load cells located near the mid height of columns recorded loads up to 16% of the total OOP load. These results attest that, in four-edges boundary conditions with perfect connection between masonry wall and RC frame, the flow-type loads are mainly transferred to the bottom beams whereas the columns attract a limited percentage of loading. This finding is compatible with the asymmetric vertical arching mechanism activated during the tests, that leads to higher shear demand on the bottom restrain. Such data are of paramount importance for the structural analysis of RC frames with masonry infill walls [18].

Since the flow depth H_w is commonly adopted as the intensity measure to define damage levels in buildings and building components, the peak capacity forces F_{OOP} recorded during the tests are converted into flow depths by means of the derived load protocols for the two considered loading conditions, as shown in Fig. 13, and results are reported in Table 5. It should be noted that, given the procedure adopted to compute the force time histories, the total applied load in z direction differs from the resultant force of the actual pressure distribution for a given H_w. The Table also reports the OOP displacement at peak capacity, recorded at a height of 0.57 m from the base of the wall. The failure of the wall is achieved at a flow depth of 1.2 m in the flood condition, and reduces to 0.9 m in the case of tsunami with a Froude number of 0.6. It is observed that the addition of plaster increases the out-of-plane deformation capacity of the tested walls by 55% (i.e. 1.4 m instead of 0.9 m). This outcome suggests that the effect of the plaster should be included in analytical models for the calculation of wall fragility under flow-type loads to avoid overestimation of their vulnerability.

To assess the effects of the flow-type loading condition on the OOP performance of masonry infill walls, results from test OOP_03 (i.e., wall with plaster under tsunami loading) are herein compared with a previous test performed on a similar specimen with the same setup under a uniform displacement distribution applied over the entire height of the wall [23]. The load protocol of such test simulates a seismic loading condition, and the displacements are applied in half cycles. The capacity curves of the two specimens are compared in Fig. 14a, whilst the crack patterns at peak capacity are compared in Fig. 14b. The peak OOP capacity of the wall with plaster under seismic loading is 61.6 kN, for an OOP displacement equal to 29.0 mm, while the recorded capacity under tsunami loading is 110.3 kN, with an OOP displacement of 4.4 mm. Such difference is justified by the activation of a different resisting mechanism, as indicated by the crack patterns at failure as shown in Fig. 14b and c. The cracking pattern for the seismic case is characterized mainly by a sub-horizontal crack at the mid height of the wall. While for a tsunami loading distribution with Fr= 0.6, the sub-horizontal crack is located above the bottom layer of bricks. This different resisting mechanism justifies the different lateral stiffness and peak capacity of the specimens under the considered loading conditions. Furthermore, the cyclic loading protocol adopted for simulating the seismic condition may lead to a slight capacity reduction with respect to a monotonic loading protocol, such as the flow-type one.

6. Updating of load-protocols

The experimental outcomes attests that the deformed shape of tested infill walls at peak capacity is asymmetrical, with high OOP displacements recorded between Line 1 and Line 2 of actuators (Fig. 10). These experimental deformed shapes, coupled with the observed bricks crushing, suggest the activation of an asymmetrical vertical thrusting arch with crack line at 0.57 m from the base of the wall.

Such observation is in contrast with the initial assumption of symmetrical arching mechanism adopted for the derivation of load time histories and protocols in Section 2.2. Based on the observed failure mode, the load protocols have been updated assuming the crack line below F_2. As such, only the protocols related to second line of actuators F_2 are updated according to the new arching scheme. The modified



Fig. 11. Experimentally observed damage vs. Field observation after the 2004 Indian Ocean Tsunami.

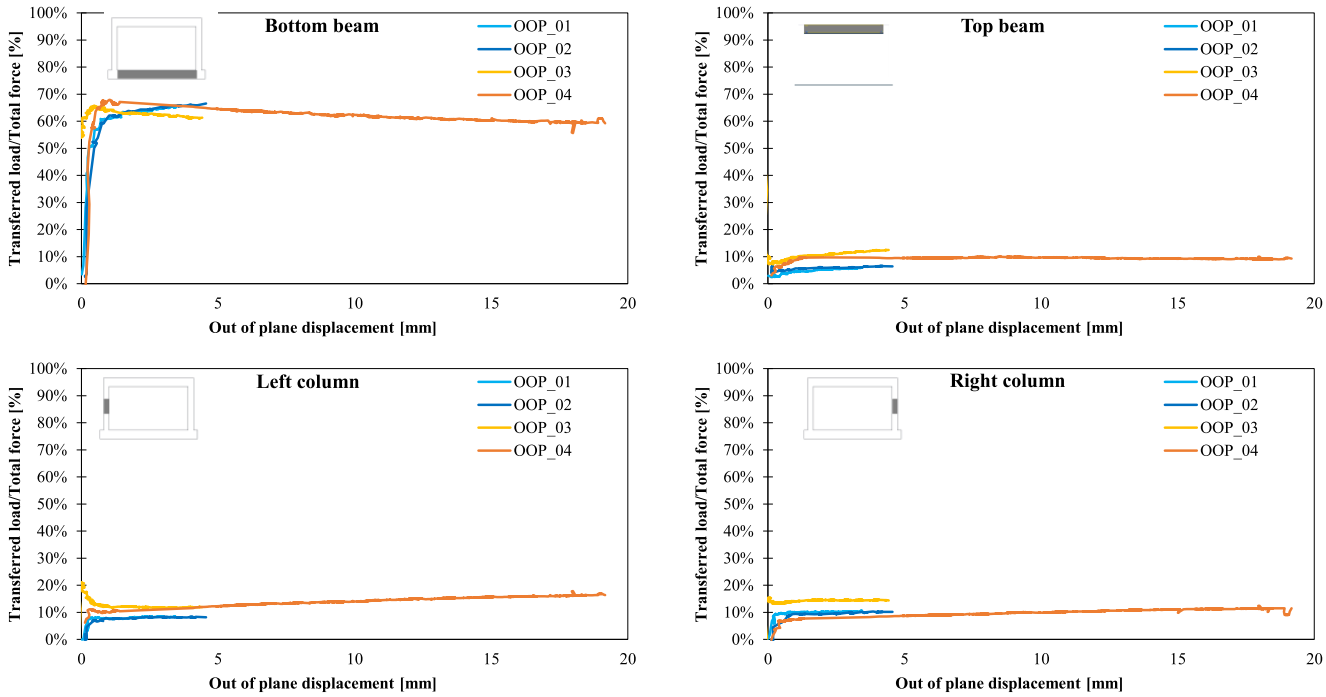

Fig. 12. Distribution of transferred OOP load from infill wall to RC beams and columns.

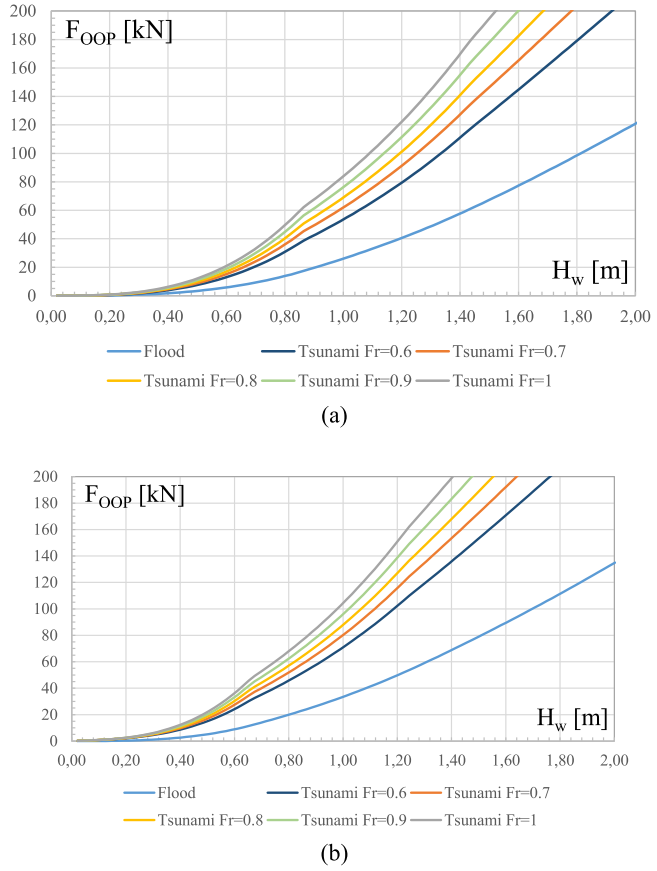

Fig. 13. Correlation charts for F_{OOP} and H_w based on the derived load protocols for Configuration 1 (a) and Configuration 2 (b).

parameters for the second line of actuators are reported in Table 6, both for setup Configuration 1 and Configuration 2. The total OOP force

Table 5
Experimental peak OOP capacity and related flow depth.

	Peak capacity [kN]	OOP displacement at peak capacity at h= 0.57 m [mm]	Flow depth at peak capacity [m]
OOP_01. Bare flood	49.9	3.5	1.2
OOP_02. Bare tsunami *Fr*= 0.6	45.9	4.5	0.9
OOP_03. Plaster tsunami *Fr*= 0.6	110.3	4.4	1.4
OOP_04. Plaster + non-structural grid tsunami *Fr*= 0.6	110.4	19.2	1.4

computed according to the initial and updated load protocols is plotted in Fig. 15 as a function of the flow depth for the loading conditions of flood and tsunami with *Fr*= 0.6 with setup Configuration 1. The comparison shows that the initial load protocols slightly overestimate the OOP loading on the infill wall for flow depths greater than 1.2 m, with increasing overestimation for increasing flow depths. For the range of OOP forces reached by the four specimens, the difference between the two load protocols appears negligible, not affecting the reliability of the tests conducted.

7. Conclusions

The study proposes a novel quasi-static testing procedure to simulate flow-type loading (i.e., hydrostatic and hydrodynamic pressure) on full-scale building components in a structural laboratory setting. The test setup is first discussed, and novel normalized load protocols are presented to implement the proposed experimental technique. The feasibility of the novel flow-type testing procedure is then demonstrated with four tests on full-scale masonry infill walls in RC frames. The walls are tested under different configurations (two bare walls, one with plaster and one with plaster and non-structural grid), providing unique experimental data on full-scale infills subjected to out-of-plane loading conditions of flood (hydrostatic load) and tsunami (combined hydrostatic

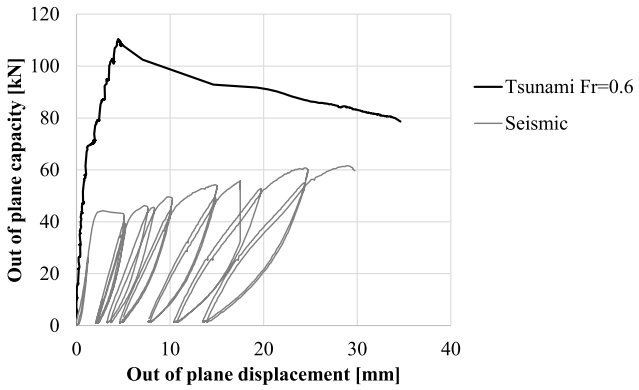

(a)

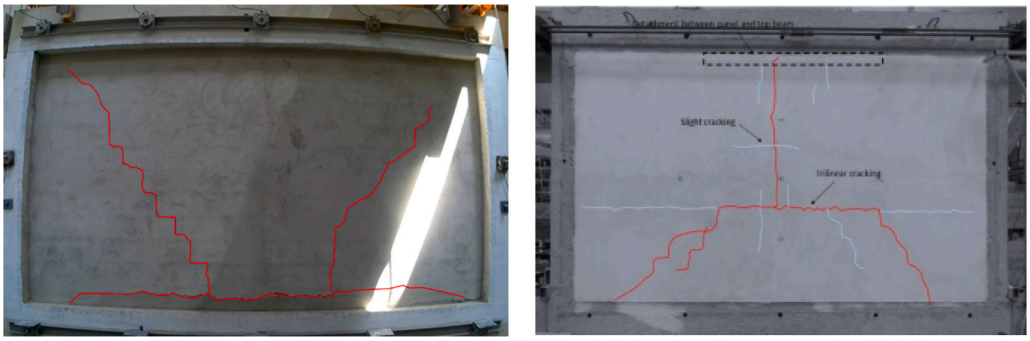

(b) (c)

Fig. 14. Seismic and tsunami capacity curves comparison (a), tsunami crack pattern (b), seismic crack pattern [23] (c).

Table 6
Updated parameters for the calculation of α_2.

	Actuators	Setup Configuration 1			Setup Configuration 2		
		λ_n	β_n	γ_n	λ_n	β_n	γ_n
Tsunami (Fr=0.6–1.0)	Second line, n = 2	0.018	0.045	0.13	0.022	0.049	0.17
Flood (hydrostatic)	Second line, n = 2	0.017	0.060	0.06	0.022	0.067	0.10

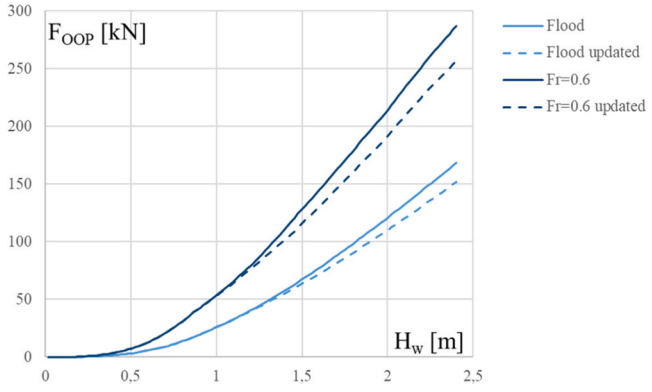

Fig. 15. Comparison between initial and updated load protocols.

and hydrodynamic loads).

Based on the outcomes of the experiments, the following conclusions can be made:

- The normalized loading protocols derived for different flow-type loading scenarios (i.e., flood and tsunami with Froude numbers from 0.6 to 1.0), provide a means of easy implementation to different control systems for the replicability of the tests;
- The OOP performance of bare masonry infill walls under flood (hydrostatic) loading and tsunami loading with *Fr*= 0.6 is quite similar in terms of peak capacity and crack pattern. This is due to the low relative contribution of the hydrodynamic force component (as compared to the hydrostatic force component), to the total lateral force. The failure mode is governed by the crushing of bricks in the bottom part of the wall, probably due to the formation of a non-symmetrical vertical arch. Once the peak capacity is achieved, the subsequent partial expulsion of the masonry and complete breakaway are caused by increasing flow depth levels. In terms of flow depth, the OOP capacity under flood is reached at 1.2 m, whereas under tsunami it reduces to 0.9 m (25% of reduction);
- The plaster (mortar only) enhanced the flexural capacity of the infill panel OOP under tsunami loading by 140% without changing the crack pattern and failure mode. The flow depth at OOP failure reached 1.4 m due to the plaster, with a 55% increase with respect to the bare wall. This suggests the need to include the effect of plaster in mechanical models for OOP capacity assessment of infill walls;
- The specimen with plaster and non-structural grid reached the same OOP capacity as the specimen with mortar only, but showed a different failure mode. In this case, the grid prevented the OOP breakaway of the wall and allowed larger OOP displacements before

failure. Such results may suggest the use of plaster with grids as a promising solution to damage reduction and contents protection during a flood or a tsunami;
- The comparison between the experimental OOP performance of infill walls tested under seismic (i.e., cyclic uniform pressure) and flow-type loading demonstrated that the loading condition significantly affects the failure mechanism and capacity of infill walls;
- The proposed experimental approach allows monitoring of the damage evolution in infill panels during a flow-type loading event, which is hard to observe in the aftermath of a flood or tsunami, where the damage condition may be representative of a series of waves of different intensities or of debris impact. Such information is of paramount importance for defining mechanical damage levels in the context of damage and loss assessment for disaster risk management, and for calibrating analytical models for vulnerability assessment.

The proposed experimental approach can be improved with high-capacity actuators to investigate tsunamis with Froude numbers greater than 0.6. This will allow the testing of different full-scale sub-assemblages, including structural components. Further experimental research may allow to investigate the effects of different loading parameters (i.e., Froude number, blocking ratio, load discretization) and properties of the walls (i.e., boundary conditions, thickness, openings, masonry type and mechanical properties). The novel setup and load protocols will allow for future experiments looking at the effect of sequential events of different intensities, such as earthquake followed by tsunami. Furthermore, experimental data will feed numerical and analytical procedures for the OOP capacity assessment of masonry infill walls under flow-type loading, to be implemented in fragility assessment frameworks.

CRediT authorship contribution statement

Marta Del Zoppo: Writing – original draft, Methodology, Data curation, Conceptualization. **José Melo:** Writing – original draft, Methodology, Data curation. **Tiziana Rossetto:** Writing – review & editing, Supervision, Methodology. **Antonio Arêde:** Writing – review & editing, Methodology. **Marco Di Ludovico:** Writing – review & editing, Methodology. **Andrea Prota:** Writing – review & editing, Methodology. **Humberto Varum:** Writing – review & editing, Supervision, Methodology.

Declaration of Competing Interest

The authors declare that they have no known competing financial interests or personal relationships that could have appeared to influence the work reported in this paper.

Acknowledgements

This project has received funding from the European Union's Horizon 2020 research and innovation programme under the Marie Skłodowska-Curie grant agreement No 101022337, awarded to Dr Marta Del Zoppo. The work of Dr. Melo, Prof. Arêde and Prof. Varum work was financially supported by: UID/04708/2025 and https://doi.org/10.54499/UID/04708/2025, of the CONSTRUCT - Instituto de I&D em Estruturas e Construções - funded by Fundação para a Ciência e a Tecnologia, I.P./ MECI, through the national funds.

Data Availability

Data will be made available on request.

References

[1] Stolle J, Goseberg N, Nistor I, et al. Debris impact forces on flexible structures in extreme hydrodynamic conditions. J Fluids Struct 2019;84:391–407.
[2] Lomonaco P, Cox D, Higgins C, et al. Building resilient coastal communities: the NHERI experimental facility for surge, wave, and tsunami hazards. Front Built Environ 2020;6:579729.
[3] Wüthrich D Ylla Arbós C, Pfister M, et al. Effect of debris damming on wave-induced hydrodynamic loads against free-standing buildings with openings. J Waterw Port Coast Ocean Eng 2020;146(1):04019036.
[4] Chandler I, Allsop W, Robinson D, et al. Evolution of pneumatic tsunami simulators – from concept to proven experimental technique. Front Built Environ 2021;7:674659.
[5] Attary N, Unnikrishnan VU, van de Lindt JW, Cox DT, Barbosa AR. Performance-based tsunami engineering methodology risk assessment of structures. Eng Struct 2017;141:676–86.
[6] Alam MS, Barbosa AR, Scott MH, Cox DT, van de Lindt JW. Development of physics-based tsunami fragility functions considering structural member failures. J Struct Eng 2018;144(3):04017221.
[7] Petrone C, Rossetto T, Goda K. Fragility assessment of a RC structure under tsunami actions via nonlinear static and dynamic analyses. Eng Struct 2017;136:36–53.
[8] Baiguera M, Rossetto T, Robertson IN, Petrone C. A procedure for performing nonlinear pushover analysis for tsunami loading to ASCE 7. J Struct Eng 2022;148(2):04021270.
[9] ASCE 7. Minimum design loads for buildings and other structures. ASCE/SEI 7-22 Rest VA 2022.
[10] Jalayer F, Carozza S, De Risi R, Manfredi G, Mbuya E. Performance-based flood safety-checking for non-engineered masonry structures. Eng Struct 2016;106:109–23.
[11] Foster ASJ, Rossetto T, Allsop W. An experimentally validated approach for evaluating tsunami inundation forces on rectangular buildings. Coast Eng 2017;128:44–57.
[12] Wüthrich D, Pfister M, Schleiss AJ. Forces on buildings with openings and orientation in a steady post-tsunami free-surface flow. Coast Eng 2020;161:103753.
[13] Xiao S, Li H. Impact of flood on a simple masonry building. J Perform Constr Facil 2013;27(5):550–63.
[14] Kabeyasawa T, Kabeyasawa T, Arikawa T, Takayama Y. Performance of soft-first-story buildings against earthquake motions and tsunami loadings. 16th World Conf Earthq 2017. 16WCEE 2017.
[15] Kabeyasawa T., Kabeyasawa T., Arikawa T.Evaluation of Tsunami Loading Based on Collapse Load of Structures. Proceedings of the Tenth Pacific Conference on Earthquake Engineering Building an Earthquake-Resilient Pacific 6-8 November 2015. Sydney, Australia.
[16] De Risi MT, Furtado A, Rodrigues H, Melo J, Verderame GM, António A, Manfredi G. Experimental analysis of strengthening solutions for the out-of-plane collapse of masonry infills in RC structures through textile reinforced mortars. Eng Struct 2020;207:110203.
[17] De Risi MT, Furtado A, Rodrigues H, Melo J, Verderame G, Arêde A, Varum H, Manfredi G. Influence of textile reinforced mortars strengthening on the in-plane/out-of-plane response of masonry infill walls in RC frames. Eng Struct 2022;254:113887.
[18] Del Zoppo M, Di Ludovico M, Prota A. Methodology for assessing the performance of RC structures with breakaway infill walls under tsunami inundation. J Struct Eng 2021;147(2):04020330.
[19] Del Zoppo M, Di Ludovico M, Prota A. A mechanics-based method towards risk assessment of RC buildings under tsunami and flow-type hazards. Eng Struct 2022;264:114452.
[20] Di Domenico M, Ricci P, Verderame GM. Experimental assessment of the influence of boundary conditions on the out-of-plane response of unreinforced masonry infill walls. J Earthq Eng 2020;24(6):881–919.
[21] Agante M, Furtado A, Rodrigues H, Arêde A, Fernandes P, Varum H. Experimental characterization of the out-of-plane behaviour of masonry infill walls made of lightweight concrete blocks. Eng Struct 2021;244:112755.
[22] Ferreira TM, Costa AA, Arêde A, Gomes A, Costa A. Experimental characterization of the out-of-plane performance of regular stone masonry walls, including test setups and axial load influence. Bull Earthq Eng 2015;13(9):2667–92 (Test masonry).
[23] Furtado. Seismic vulnerability assessment and retrofitting strategies for masonry infilled frame buildings considering in-plane and out-of-plane behaviour. PhD thesis.
[24] Furtado A, Rodrigues H, Arêde A, Melo J, Varum H. The use of textile-reinforced mortar as a strengthening technique for the infill walls out-of-plane behaviour. Compos Struct 2021;255:113029.
[25] CEN. EN 1998-3 Eurocode 8: design of structures for earthquake resistance, part 3: assessment and retrofitting of buildings. European Committee for Standardization; 2005.
[26] Furtado A, Rodrigues H, Arêde A, Varum H. Mechanical properties characterization of different types of masonry infill walls. Front Struct Civil Eng 2020;14(2):411–34.
[27] CEN. EN 1052-1. Methods of Test for Masonry, Part 1: Determination of Compressive Strength. London: British Standards Institution; 1998.
[28] Furtado A, Rodrigues H, Arede A, Varum H. Experimental investigation on the possible effect of previous damage, workmanship and test setup on the out-of-plane behaviour of masonry infill walls. J Earthq Eng 2022;26(11):5647–78.
[29] Del Zoppo M, Wijesundara K, Rossetto T, Baiguera Dias, P, Di Ludovico, M M, Prota A. Influence of exterior infill walls on the performance of RC frames under

tsunami loads: Case study of school buildings in Sri Lanka. Eng Struct 2021;234:111920.

[30] Saatcioglu M, Ghobarah A, Nistor I. Effects of the December 26, 2004 Sumatra earthquake and tsunami on physical infrastructure. ISET J Earthq Technol 2005;42(4):79–94.

[31] Ghobarah A, Saatcioglu M, Nistor I. The impact of the 26 December 2004 earthquake and tsunami on structures and infrastructure. Eng Struct 2006;28(2):312–26.